REPORT

A full solid-state conceptual magnetocaloric refrigerator based on hybrid regeneration

Yuan Lin,[1,2] Jing Wang,[1,2,*] Wei Dai,[3] Kaiming Qiao,[1] Houbo Zhou,[1,2] Tongyun Zhao,[1,5] Fengxia Hu,[1,2,4,*] and Baogen Shen[1,2,6,*]
*Correspondence: wangjing@iphy.ac.cn (J.W.); fxhu@iphy.ac.cn (F.H.); shenbg@iphy.ac.cn (B.S.)
Received: March 5, 2024; Accepted: May 19, 2024; Published Online: May 22, 2024; https://doi.org/10.1016/j.xinn.2024.100645

GRAPHICAL ABSTRACT

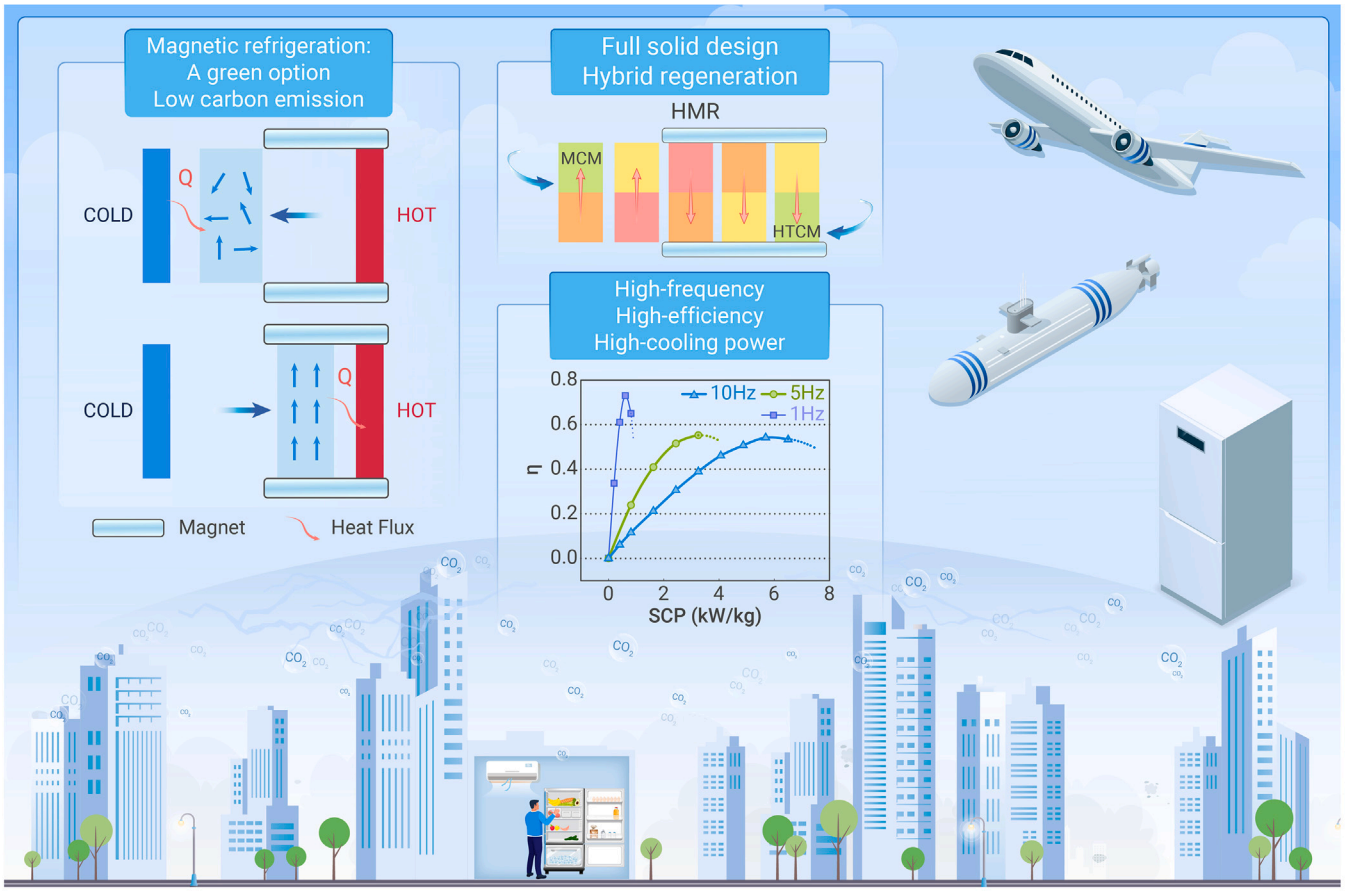

PUBLIC SUMMARY

- Magnetocaloric refrigeration is highly efficient and environmentally benign compared to vapor compression refrigeration.
- Unlike traditional active/passive regenerators where a stable temperature gradient only exists in magnetocaloric or heat transfer materials, the newly proposed hybrid regenerator generates a stable temperature gradient in both parts, effectively improving cooling efficiency.
- Full solid-state design overcomes the frequency limitation set by fluid in traditional magnetocaloric refrigerators, significantly improving working frequency and cooling power.
- The presented full solid-state hybrid regeneration device can realize high-frequency, high-efficiency, and high-cooling power refrigeration.

REPORT

A full solid-state conceptual magnetocaloric refrigerator based on hybrid regeneration

Yuan Lin,[1,2] Jing Wang,[1,2,*] Wei Dai,[3] Kaiming Qiao,[1] Houbo Zhou,[1,2] Tongyun Zhao,[1,5] Fengxia Hu,[1,2,4,*] and Baogen Shen[1,2,6,*]

[1]Beijing National Laboratory for Condensed Matter Physics, Institute of Physics, Chinese Academy of Sciences, Beijing 100190, China

[2]School of Physical Sciences, University of Chinese Academy of Sciences, Beijing 101408, China

[3]Key Laboratory of Cryogenics, Technical Institute of Physics and Chemistry, Chinese Academy of Sciences, Beijing 100190, China

[4]Songshan Lake Materials Laboratory, Dongguan 523808, China

[5]Ganjiang Innovation Academy, Chinese Academy of Sciences, Ganzhou 341000, China

[6]Ningbo Institute of Materials Technology & Engineering, Chinese Academy of Sciences, Ningbo 315201, China

*Correspondence: wangjing@iphy.ac.cn (J.W.); fxhu@iphy.ac.cn (F.H.); shenbg@iphy.ac.cn (B.S.)

Received: March 5, 2024; Accepted: May 19, 2024; Published Online: May 22, 2024; https://doi.org/10.1016/j.xinn.2024.100645

Citation: Lin Y., Wang J., Dai W., et al., (2024). A full solid-state conceptual magnetocaloric refrigerator based on hybrid regeneration. The Innovation **5(4)**, 100645.

The environmental friendliness and high efficiency of magnetocaloric refrigeration make it a promising substitute for vapor compression refrigeration. However, the common use of heat transfer fluid in conventional passive magnetic regenerators (PMRs) and active magnetic regenerators (AMRs) makes only partial materials contribute to the regeneration process, which produces large regeneration loss and greatly limits the regeneration efficiency and refrigeration performance at high frequency. Herein, we propose a new conceptual hybrid magnetic regenerator (HMR) composed of multiple solid-state high thermal conductivity materials (HTCMs) and magnetocaloric materials (MCMs), in which both HTCM and MCM elements participate in the regeneration process. This novel working mode could greatly reduce regeneration losses caused by dead volume, pressure losses, and temperature nonuniformity in heat transfer substances to markedly improve regeneration efficiency at high working frequencies. Using the experimentally obtained adiabatic temperature change and magnetic work and with the help of finite element simulation, a maximum temperature of 26 K, a dramatically large cooling power of 8.3 kW/kg, and a maximum ideal exergy efficiency of 54.2% are achieved at the working frequency of 10 Hz for an ideal prototype device of a rotary HMR magnetocaloric refrigerator, which shows potential for achieving an integrative, advanced performance against current AMR/PMR systems.

INTRODUCTION

The vapor compression (VC) refrigerator has dominated the modern cooling market with the prioritization of mature production and design technology and with outstanding overall performances after nearly two centuries of development.[1,2] It has been reported that approximately one-tenth of global electricity consumption is spent on refrigeration, and the energy consumed by cooling equipment is estimated to more than triple by 2050.[3] However, the cooling efficiency of VC refrigerators has yet to achieve satisfactory performance,[4,5] leading to energy waste. Furthermore, typical refrigerants used in VC refrigerators, such as hydrofluorocarbons, often have a global warming potential exceeding 1,000.[6,7] Additionally, the use of compressors hinders the use of VC refrigerators in miniaturized refrigeration for electronics.

With high efficiency, solid-state caloric refrigeration, including magnetocaloric (MC), electrocaloric, elastocaloric, and barocaloric refrigeration,[8-20] is acknowledged as a promising candidate to substitute traditional VC cooling. The refrigerants used in these types of caloric refrigeration are solid caloric materials, which exhibit a reversible entropy change during a phase transition triggered by an external field, introducing zero ozone depletion potential and an extremely low global warming potential.[21,22] Thereinto, the high thermal conductivity and cycling stability of MC materials (MCMs) make the refrigeration process more readily in MC refrigeration.

Since the discovery of a series of new giant MCMs, such as GdSiGe, $La(Fe,Si)_{13}$, etc.,[23-25] a lack of a subtle design of MC prototypes has become a bottleneck to the wider application of MC refrigeration. Brown proposed the first room temperature MC refrigerator based on a passive magnetic regenerator (PMR), which required a temperature gradient in heat transfer substances (e.g., gas or liquid) (Figure 1A),[26] where the small volume ratio of the MCM to the device severely limited its specific cooling power (SCP). As an improvement, Barclay and Steyert introduced an active magnetic regenerator (AMR) into an MC refrigerator[27] in which MCMs took part in both the cooling and regeneration processes and thus experienced an extra temperature gradient, and no stable temperature gradient existed in the heat transfer substance (Figure 1B). This behavior lowered the portion of ineffective substances and improved the SCP. Owing to this feature, the AMR was widely used in subsequently reported MC refrigerators, and impressive progress has been achieved.[21,28-30] However, the SCP and exergy efficiency (η) of these AMR refrigerators are still far from theoretically predicted limits. One key reason for this is that almost all established AMR refrigerators use fluid to transfer heat, which introduces unavoidable regeneration losses from dead volume, pressure losses, and unwanted heat transfer caused by the temperature nonuniformity in the heat transfer substances during operation.[31] Furthermore, the slow-moving speed and low thermal conductivity of the fluid limit the working frequency, causing a restriction of the SCP.[21,28]

To overcome these disadvantages, new designs of full solid-state MC refrigerators using Peltier elements,[32] k_H materials (whose thermal conductivity is influenced by magnetic fields),[33] or high thermal conductivity materials (HTCMs)[34] to carry the regeneration process came into sight.[31] These designs show abilities to reduce the influence of dead volume and pressure losses and break the restriction of the working frequency but still face respective deficiencies. For example, k_H materials are difficult to obtain, while Peltier elements usually introduce an additional external driving power. Additionally, employing a single HTCM slice with a big size to carry the regeneration process inevitably results in temperature nonuniformity, which aggravates the regeneration losses.[35,36] A common problem of these full solid-state prototypes is that the regeneration loss from the temperature nonuniformity cannot be effectively reduced.

Here, we propose a new hybrid magnetic regenerator (HMR) based on combining the principles of PMRs and AMRs, in which a stable temperature gradient is generated in both the heat transfer substance and MCM and both parts participate in the regeneration cycle (Figure 1C). On the basis of this new regeneration system, we present a full solid-state rotary HMR refrigerator employing multiple discrete HTCM and MCM slices to realize regeneration, in which various regeneration losses can be effectively reduced and the frequency limitation can be broken. Additionally, this MC refrigerator is scalable.[29]

In this paper, the structure and working principle of the HMR refrigerator are first introduced. Second, we discuss how, based on the experimentally measured adiabatic temperature change (ΔT_{ad}) and magnetic work (W_m) of MCMs (Gd, $La(Fe,Si)_{13}$), as well as the related parameters of MCMs (Gd, $La(Fe,Si)_{13}$) and HTCMs (Cu, Ag, aluminum-diamond alloy [ALC]),[37-40] finite element simulations were performed with COMSOL Multiphysics 5.6 to investigate the performance of the present HMR refrigerator (supplemental information S1; Video S1). The outer radius of the devices was 10 mm, and the total thickness of the core refrigeration unit was approximately 0.3 mm. This HMR prototype exhibits excellent refrigeration performance over a wide frequency range (from 0.1 to 10 Hz): especially at 10 Hz, a maximum temperature of 26 K, a maximum cooling power of 8.3 kW/kg, and a maximum η of 54.2% are achieved from the combination of Gd and Cu in an ideal prototype, which shows the potential to produce an integrative, advanced performance against current AMR/PMR systems. Finally, by evaluating the performance of different HTCMs (Cu, Ag, ALC) and MCMs (Gd, $La(Fe,Si)_{13}$), we provide guidance for

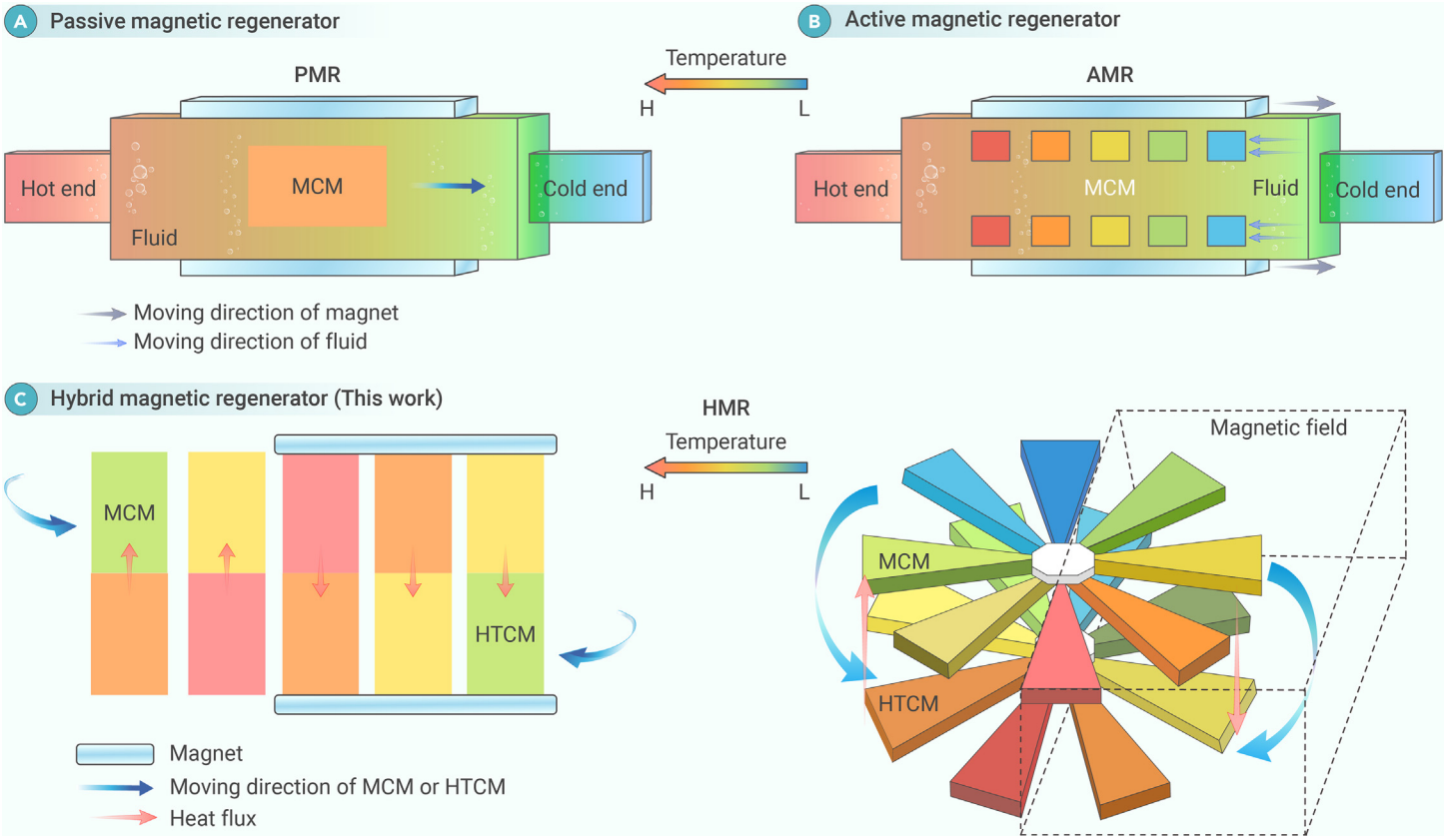

Figure 1. Schematic diagram of the working principle for three regeneration modes (A) PMR, (B) AMR, and (C) HMR.

selecting materials in full solid-state prototypes and exploring favorable materials for HMR refrigerators.

Model and working principle

Figure 2 illustrates the device configuration and working principle of the proposed HMR MC refrigerator (slice number [*Ns*] = 8 for example). The core of the system comprises two stacked layers: a cooling layer (CL) made of MCMs and a regeneration layer (RL) made of HTCMs. Each layer is divided into *Ns* sectors, and the gap between two sectors in each layer is composed of adiabatic materials, i.e., low thermal conductivity materials, whose area is equal to the sector. In other words, the CL (RL) is equally separated into 2 *Ns* parts: half of that is made of MCMs (HTCMs) and the other half is made of adiabatic materials to block the heat transfer in the same layer (see Figure 2A), leading to the formation of a stable temperature gradient in the layer. The RL and CL rotate coaxially at the same angular speed but in opposite directions, as indicated by the arc-shaped arrows in Figure 2B. During the rotation, the neighboring MCM and HTCM sectors in proximate layers are in direct contact to facilitate heat transfer (see Figure 2B). A temperature-entropy plot, which illustrates the Brayton cycle (two isentropy and two iso-field processes) experienced in MCMs during the cooling process, is shown in Figure 2D. Additionally, two more sectors on top of C5 and C1, as shown in Figures 2A–2C, play the role of cold and hot ends, respectively, to exhibit the refrigeration performance of the MC refrigerator. In practice, the design of hot and cold ends will depend on the specific requirements.

A magnetic field can be applied to each MCM sector with the rotation of the CL. For the CL, half of the layer is placed under the magnetic field, and the other half is located at a zero-field region, as shown in Figure 2C (supplemental information S12). As the CL rotates through the hot end and enters the magnetic field counterclockwise, each MCM sector experiences an adiabatic temperature increase during the rotation from C8 to C1 (stage C shown in Figure 2D) and then releases heat during the rotation from C1 to C4 (stage D) to the HTCM sectors of the RL, which approach clockwise in sequence (from R4 to R1) at the region with the magnetic field (see Figure 2C). As a result, the temperature of the MCM (HTCM) sector gradually decreases (increases) during the rotation under the magnetic field. At the same time, the MCM sector at the cold end (see Figure 2C) leaves the magnetic field counterclockwise from C4 to C5 (stage A), experiencing an adiabatic temperature decrease, and then absorbs heat (from C5 to C8, stage B) from the HTCM sectors (from R5 to R8) at the zero-field region. This results in a gradual temperature increase in the MCM and a decrease in the HTCM during the rotation in the zero-field region.

To conclude, in the field half, the RL absorbs heat from the CL, and in the other half, the RL releases heat to the CL, which means that the heat rejected by the CL at the field half is absorbed by the CL at the other half (red arrows in Figure 2D), thus realizing regeneration with the coactions of the CL and RL. A temperature gradient is built in both the CL and RL owing to the heat exchange between them. In each cycle, the MCM (HTCM) sector reaches the lowest (highest) temperature at the cold (hot) end just after (before) leaving the magnetic field counterclockwise (clockwise) and the highest (lowest) temperature at the hot (cold) end after (before) entering the magnetic field. Through such a cycle, heat is transferred from the cold end to the hot end, realizing a temperature span (ΔT_{span}; defined as the difference between hot and cold end temperature) much larger than the ΔT_{ad} of the MCM element.

As is known, PMRs and AMRs usually have a temperature gradient in the heat transfer substances or MCMs, respectively, which means that only the heat transfer or the MCM part contributes to the regeneration process. However, in the proposed HMR, stable temperature gradients appear in both parts, such that the whole device participates in the regeneration cycle, which nearly eradicates the regeneration loss caused by the temperature nonuniformity, realizing high-efficiency regeneration and refrigeration. Moreover, the volume of the HTCMs in this device is comparable to that of the MCMs, minimizing the heat losses introduced by the ineffective spare contact between the MCMs and HTCMs. Finally, the full solid design and the use of HTCMs could eliminate heat losses from dead volume and pressure losses, as well as break the frequency restriction aroused by the fluid used in most reported AMR refrigerators. Additionally, this device can be scaled along the diameter, from meters to millimeters, or stacked along the thickness direction (supplemental information S11) to fulfill the refrigeration demands of different-size targets, such as electronics and buildings.

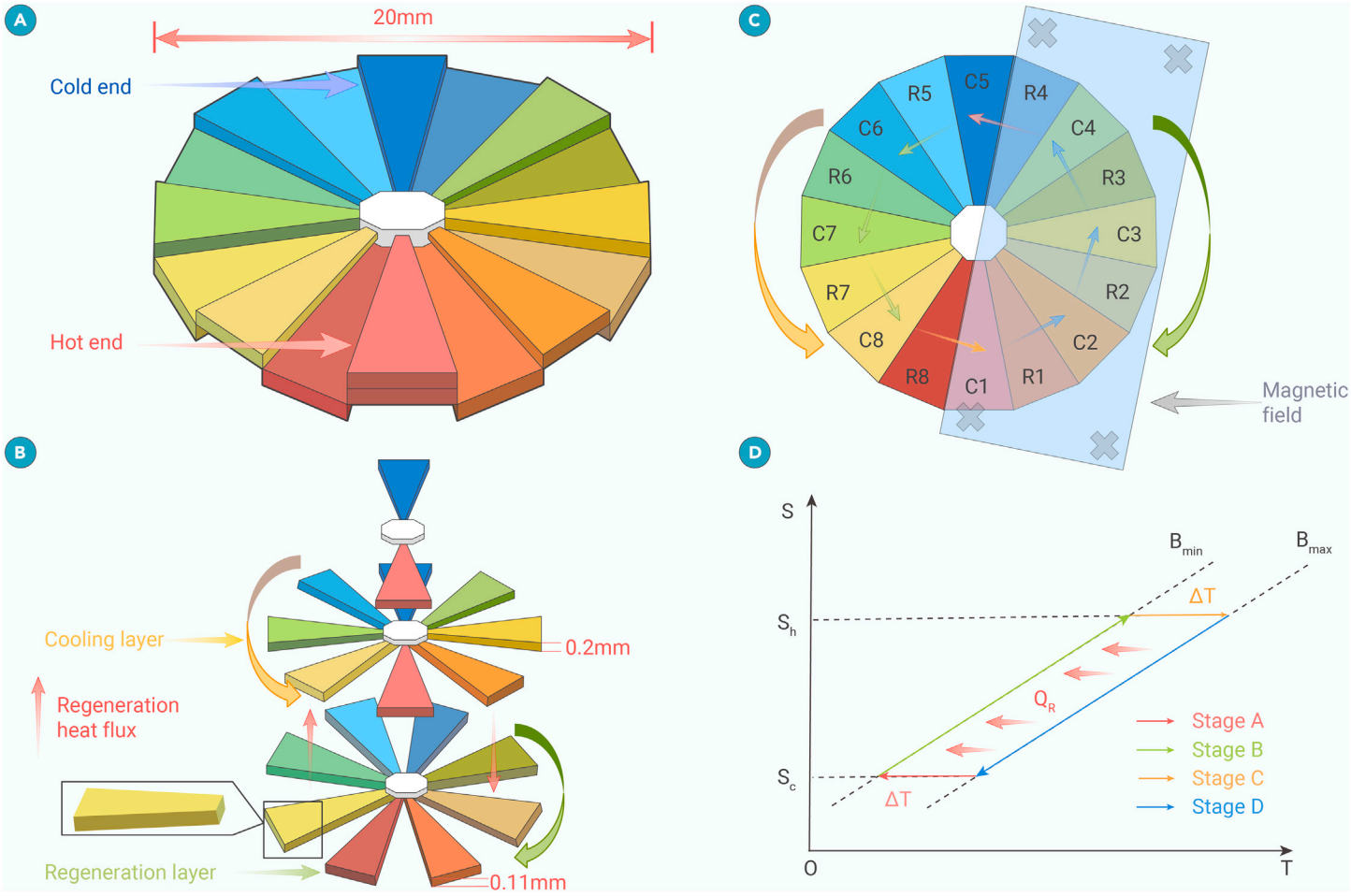

Figure 2. Structure and working principle of the HMR refrigerator (A and B) The (A) compact and (B) split sketches of the refrigerator (*Ns* = 8 for example). (C and D) The working principle of the refrigerator is shown in (C) the top view (*Ns* = 8) and (D) temperature-entropy diagram (Brayton cycle). In simulations, the inner and outer radii of the investigated devices were 1 and 10 mm, respectively, while the CL thickness was set as 0.1 or 0.2 mm and the RL thickness ranged from 0.09 to 0.18 mm.

RESULTS AND DISCUSSION

Optimization of the structure parameters

As mentioned earlier, the performance of the refrigerator is closely related to the regeneration process, which is determined by the heat exchange efficiency between the CL and RL during their relative rotation. Deploying Gd and Cu as the MCM and HTCM, respectively, a serial of devices was built to explore the optimal structure parameters. In practice, considering convenience and costs, the magnetic field used for MC refrigeration usually ranges from 0.8 to 1.3 T. Hence, a field of 1.35 T was chosen here to demonstrate the performance a device might achieve in practical applications. From the M-H measurements by SQUID-VSM, the entropy change and the ΔT_{ad} of Gd were calculated as a function of the temperature (see supplemental information S5 and S7 and Figures S4 and S6). The ΔT_{ad} of Gd in the simulation was set as 4 K @ 1.35 T based on the measured results. By analogy with the AMR mode, the utilization factor (U_f), which represents the heat capacity of the HTCMs to that of the MCMs, was used to quantify the operation of our HMRs (Equation 1, where ρ, t, and C denote the density, thickness, and specific heat capacity of the CL or RL, respectively):[41]

$$U_f = \frac{\rho_{HTCM}\, t_{HTCM} C_{p,HTCM}}{\rho_{MCM}\, t_{MCM} C_{p,MCM}}. \quad \text{(Equation 1)}$$

The temperature span between the hot and cold ends, ΔT_{span}, was evaluated for the device under no extra cooling load. The number of CL/RL sectors was set to be *Ns* = 24, where the thickness of the CL (Gd) was fixed at 0.2 mm, and the results are shown in Figure 3A. A maximum ΔT_{span} of 47 K (at 1 Hz) is obtained at a U_f of ~1.0 (d_{RL} = 0.11 mm, d_{CL} = 0.2 mm), which indicates that a compromise in the relative heat capacity of the regeneration element is required for an efficient heat transfer. During each heat transfer progress, an RL with a smaller heat capacity (relative to the CL) cannot absorb sufficient heat from the CL at the field half (see Figure 2C), whereas an RL with a larger heat capacity would make the heat release (from the RL to the CL) insufficient at the zero-field half. Obviously, the mismatch in the heat capacities of RL and CL sectors reduces the efficiency of regeneration and leads to a lower ΔT_{span}. As a result, an optimal U_f emerges for an HMR refrigerator with the given RL and CL materials. More importantly, it was found that the optimal U_f stays almost the same (~1.0) with a varying working frequency from 1 to 10 Hz (see Figure 3A), indicating that the optimal U_f of the proposed HMR refrigerator is insensitive to the working frequency. This unique characteristic is largely related to the distinctive temperature gradient in both the RL and CL sectors and shows the clear technological superiority of the HMR mode over the AMR, in which the optimal U_f largely declines when the frequency increases.[41] This means that our new HMR refrigerator could work at a much higher frequency than AMR or PMR devices, whose desired operating frequency is often much less than 1 Hz.[28,41]

On the other hand, ΔT_{span} is also determined by the *Ns*. Figure 3B illustrates the ΔT_{span} and regeneration factor (R_f, defined as $R_f = \Delta T_{span}/\Delta T_{ad}$) versus *Ns* at the optimal U_f of 1.0. For a given frequency, a larger *Ns* leads to a larger ΔT_{span} and R_f. The ability to regulate R_f in this device is of great interest for developing practical MC refrigerators. At 1 Hz, ΔT_{span} rises almost linearly with the *Ns*, reaching 59 K at *Ns* = 32. Accordingly, the R_f is approximately half the *Ns* value, reaching 14.8 at *N* = 32. Notably, when the frequency is increased, R_f deviates from a linear dependency on *Ns* and decreases at higher *Ns* (6.9 at *N* = 32 and 10 Hz), indicating a negative impact of the working frequency on the regeneration progress increases with the *Ns*.

Characteristic of working frequency

Figure 3C shows the evolution of maximum ΔT_{span} (*Ns* = 24) with the working frequency at the optimal $U_f \approx 1.0$ (d_{RL} = 0.11 mm, d_{CL} = 0.2 mm). It was found that

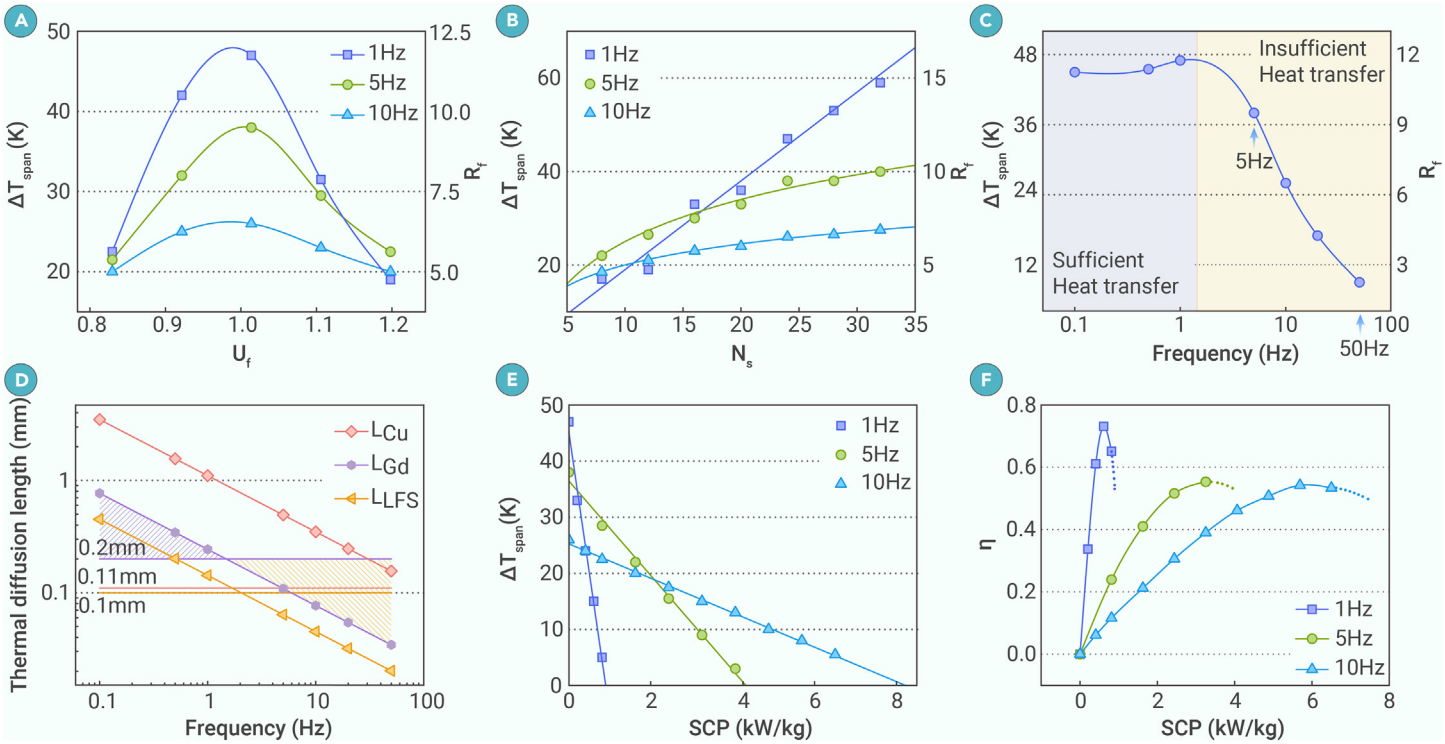

Figure 3. Impact of structural parameters and frequency on refrigeration performance of Gd-Cu (A) Temperature span (ΔT_{span}) and regeneration factor (R_f) versus utilization factor (U_f) at different working frequencies. (B) ΔT_{span} and R_f as a function of *Ns* for different working frequencies at an optimal U_f of 1.0. (C) Evolution of the ΔT_{span} and R_f with working frequency for a U_f of 1.0. (D) Frequency evolution of the thermal diffusion length of MCM-Gd, MCM-LFS, and HTCM-Cu elements, where the horizontal lines denote the element thickness of the investigated devices for Cu, Gd, and LFS. The purple and orange shaded areas in (C) and (D) denote the frequency areas where the heat transfer is sufficient and insufficient, respectively. (E and F) ΔT_{span} (E) and exergy efficiency (η; F) versus specific cooling power (SCP) for different frequencies at a fixed U_f = 1.0. The dashed lines in (F) are a guide for the eyes.

ΔT_{span} is stable when the working frequency is lower than 1 Hz but decreases sharply for frequencies larger than 1 Hz. The decline of ΔT_{span} at high working frequencies may arise from insufficient heat exchange between the MCM and HTCM elements. In our device, the regeneration process of the device is mainly fulfilled through heat exchange along the z direction between neighboring MCM and HTCM elements, which is strongly affected by both the thickness and thermal diffusion length of the MCM or HTCM. When the thickness d_{MCM} (or d_{HTCM}) is larger than the thermal diffusion length L_{MCM} (or L_{HTCM}), the heat exchange between MCMs and HTCMs is insufficient, resulting in a lower ΔT_{span}. Usually, the diffusion length (L) can be calculated from the following equation:[12]

$$L = \sqrt{\alpha * \Delta t} = \sqrt{\frac{\kappa}{\rho * c} * \Delta t} = \sqrt{\frac{\kappa}{\rho * c} * \frac{1}{96 * f}} \qquad \text{(Equation 2)}$$

where α is the thermal diffusivity, Δt is the heat exchange time, κ is the thermal conductivity, ρ is the density, c is the specific heat capacity at constant pressure, and f is the working frequency. Figure 3D compares the thermal diffusion length of MCMs and HTCMs at various working frequencies. One can find that the thermal diffusion length of HTCM Cu is always larger than the optimized thickness at frequencies lower than 50 Hz (see the red lines in Figure 3D; $L_{Cu,50Hz}$ = 0.156 mm > d_{Cu} = 0.11 mm), suggesting that the heat transfer in HTCM elements for the calculated frequencies is always sufficient. Thus, only the restriction of MCMs on ΔT_{span} needs to be considered in our case. For MCM Gd, simple calculations can get $L_{Gd,5Hz} < d_{Gd} = 0.2$ mm $< L_{Gd,1Hz}$ ($L_{Gd,5Hz}$ = 0.109 mm, $L_{Gd,1Hz}$ = 0.24 mm), as shown in Figure 3D. Obviously, for a frequency higher than 1 Hz (the orange shaded area), the heat transfer in the MCM element of Gd and thus the exchange between MCMs and HTCMs are insufficient, causing the dive of ΔT_{span}, as shown in Figure 3C, while for a frequency lower than 1 Hz (the purple shaded area), it is sufficient to maintain the ΔT_{span}.

Refrigeration performance

The refrigeration performance of the system, including the cooling power and the η (η = coefficient of performance [COP]/COP_{carnot}), was further investigated in a device with an optimal U_f (d_{RL} = 0.11 mm, d_{CL} = 0.2 mm) and *Ns* of 24. The hot-end temperature was fixed at room temperature as the initial temperature (see Figure S3 and supplemental information S4), and various loads were applied at the cold end to evaluate the refrigeration efficiency. Without loss of generality, the COP of the proposed refrigerator is defined as the ratio between the cooling capacity (Q_c) and the work performed by the magnetic field per cycle:

$$COP = \frac{Q_c}{W_m} = \frac{Q_c}{N_s \int_{T_c}^{T_H} MdH}, \qquad \text{(Equation 3)}$$

where Q_c is the cooling capacity of the system and T_H and T_C are the temperatures of the hot end and cold end, respectively. The W_m was calculated based on the M-H curves measured by the SQUID-VSM. The calculation of COP is shown in supplemental information S2 and Figure S1. The η[21,42] is defined by

$$\eta = \frac{COP}{COP_{carnot}} = COP \times \frac{(T_H - T_C)}{T_C}. \qquad \text{(Equation 4)}$$

Figures 3E and 3F present the ΔT_{span} and η as a function of SCP for different operating frequencies (supplemental information S10). First, the ΔT_{span} at the no-load condition decreases by nearly a half (from 47 to 26 K) when the frequency increases from 1 to 10 Hz (see the vertical intercept in Figure 3E). Additionally, η decreases with increasing frequency at a given SCP (Figure 3F), showing a maximum value of 73.1% at 1 Hz. This result suggests that the refrigeration efficiency is better at low frequency, which is attributed to the complete heat exchange between the MCM and HTCM sectors. Conversely, the operating frequency has a positive impact on the available cooling power (see Figure 3F and the transverse intercept in Figure 3E). For a given ΔT_{span}, the cooling power increases with the frequency until the duration of the contact between MCM and HTCM sectors becomes insufficient for effective heat exchange. Moreover, ΔT_{span} decreases linearly with SCP at all frequencies, indicating no extra refrigeration consumption during the regeneration process. This should be attributed to the full heat contact between MCM and HTCM slices and the unique temperature gradient character of HMRs, which avoids heat losses from the dead volume and

Table 1. Performance comparison of present HMR modes with other MC refrigerators based on typical PMR or AMR

Type	Country	Frequency (Hz)	$\Delta T_{span\text{-}max}$ (K)	SCP_{max} (kW/kg)	η (%)	Magnetic field (T)	Ref.
PMR model							
PMR/reciprocating, Gd plates/liquid (experiment)	USA	–	47	–	–	7	Brown et al.[26]
AMR model							
AMR/rotary, Gd spheres/ liquid (experiment)	Canada	4	29	0.91	4.3	1.5	Tura et al.[43]
AMR/rotary, Gd spheres/ liquid (experiment)	Denmark	2	25.4	0.36	5.6	1.24	Engelbrecht[44]
AMR/reciprocating, Gd plates/ liquid (experiment)	Spain	0.2	3.5	0.02	–	1	Romero Gomez et al.[45]
AMR/rotary, LaFeSiH alloys/ liquid (experiment)	USA	4	18	2.0	7	1.44	Jacobs et al.[46]
AMR/reciprocating, Gd particles/ He gas (experiment)	China	1	42	0.04	–	1.5	Yao et al.[47]
AMR/rotary, Gd plates/liquid (simulation)	Italy	2.6	35	0.25	28	1	Bocanegra et al.[48]
AMR/reciprocating, Gd plates/ liquid (simulation)	Italy	0.22	15	0.13	27.7	2	Aprea et al.[49]
AMR/reciprocating, Gd particles/ liquid (simulation)	China	0.11	3	0.29	13.2	2.18	Liu et al.[50]
AMR/rotary, GdPd plates/ liquid (simulation-experiment)	Italy	0.5	30	0.26	33	1.5	Tagliafico et al.[51]
AMR/reciprocating, Gd plates/ liquid (simulation)	Switzerland	0.33	27	-	26.9	1.5	Chiba et al.[52]
HMR model (this work) (simulation-experiment)	China	–	–	–	–	–	–
HMR/rotary, 0.2 mm Gd/ 0.11 mm Cu slices	proposed system	1	47	0.9	73.1	1.35	this work
HMR/rotary, 0.2 mm Gd/ 0.11 mm Cu slices	proposed system	5	38	4.3	55.3	1.35	this work
HMR/rotary, 0.2 mm Gd/ 0.11 mm Cu slices	proposed system	10	26	8.3	54.2	1.35	this work
HMR/rotary, 0.1 mm LFS/ 0.13 mm Cu slices	proposed system	10	14	9.8	53.3	1.35	this work
HMR/rotary, 0.2 mm Gd/10 nm air gap/0.11 mm Cu slices[a]	proposed system	10	24	7.8	52.4	1.35	this work
HMR/rotary, 0.2 mm Gd/100 nm air gap/0.11 mm Cu slices[a]	proposed system	10	16.5	7.3	40.0	1.35	this work

LFS denotes $La(Fe_{0.92}Co_{0.08})_{11.7}Si_{1.3}$. "Experiment" and "simulation" mean that the results were obtained by experiment or simulation, respectively, while "simulation-experiment" means that the results were obtained by combining simulation with the experimentally measured adiabatic temperature change and magnetic work of MCMs.

[a]Device with an air gap aimed at solving friction (if assuming that ballistic transport plays a dominant role, then a small pressure applied in the air gap could help to obtain a similar cooling performance; see supplemental information S9).

temperature inhomogeneity inside the MCM/HTCM elements. This effect effectively improves the regeneration efficiency and further increases the available cooling power at high frequency. As a result, a maximum ΔT_{span} of 26 K, a dramatically large cooling power of 8.3 kW/kg, and a maximum η of 54.2% are achieved at 10 Hz for the combination of Gd and Cu. It should be noted that at high frequencies, the friction between the two layers may produce extra heat and wear the surface, potentially neutralizing the cooling performances and damaging the device. To minimize the influence of friction, as an alternative to thermal grease, an air gap may be introduced between the two layers. When the thickness of the introduced air gap is 10 nm, at 10 Hz, the cooling performance remains nearly unchanged; when introducing an air gap of 100 nm, the maximal cooling power decreases by 13% from 8.3 to 7.2 kW/kg, and the maximal Carnot efficiency decreases by 26% from 54% to 40%. That is to say, by introducing an air gap below 100 nm, the friction issue could be addressed while maintaining the excellent cooling performance (Table 1; if assuming that ballistic transport plays a dominant role, then a small pressure applied in the air gap could help to obtain a similar cooling performance; see supplemental information S9).

Moreover, to practically demonstrate the influence of friction on the cooling performance, we simply tested the influence of friction through relative motion of Gd and Cu slices, where the hybrid regeneration principle is exactly the same as the rotary one. With all the nonideal conditions like friction, air convection, and surface thermal resistance existing, utilizing two miniaturized Gd slices of 3 × 10 × 1 mm and three Cu slices of 3 × 5 × 1 mm, a ΔT_{span} of ~4.6 K formed in tens of seconds at approximately 0.5 Hz. However, the imbalance of the increase of the hot end (~2.6 K) and the decrease of the cold end (~2 K) demonstrates the influence of friction. To further test the specific influence of friction, we removed the permanent magnet and operated the device at zero field and approximately 0.5 Hz. Because of the friction, the temperature of the hot end increased by approximately 0.15 K, and the influence was

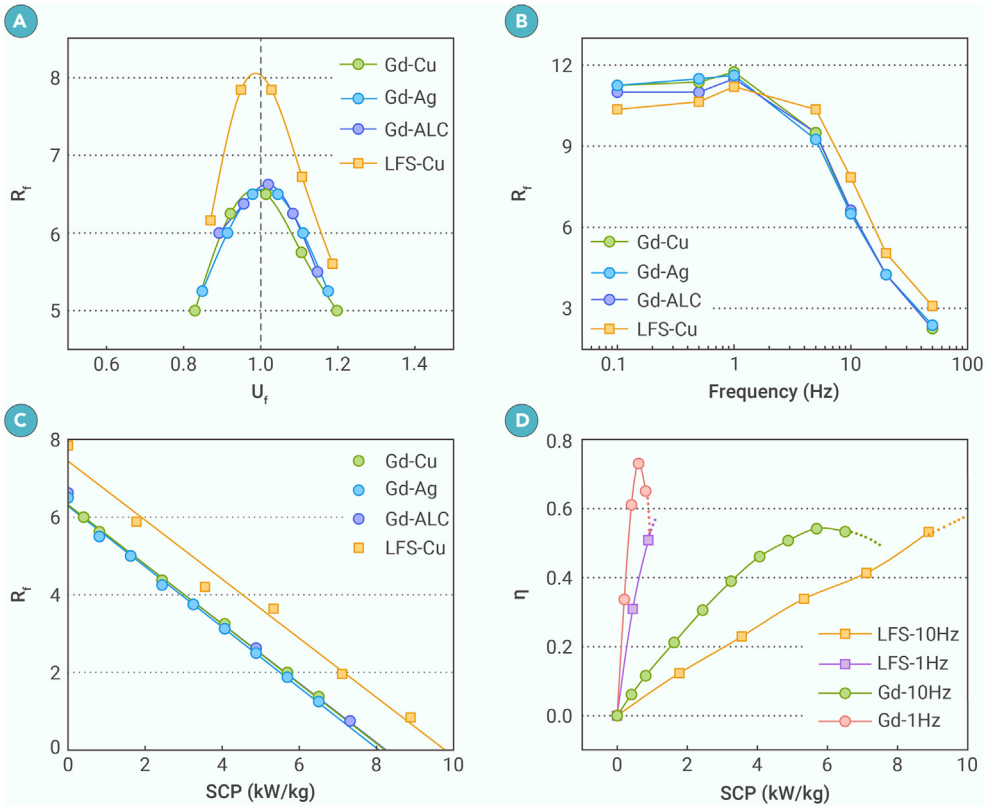

Figure 4. Comparison of the refrigeration performances of different MCMs and HTCMs (A) R_f versus U_f for devices composed of different MCMs and HTCMs at a working frequency of 10 Hz and zero cooling load. (B) R_f versus working frequency for devices composed of different MCM and HTCM elements at zero cooling load. (C) R_f versus SCP for devices composed of different MCM and HTCM elements at a working frequency of 10 Hz. (D) η versus SCP for devices with Gd-MCM and LFS-MCM at frequencies of 1 and 10 Hz, respectively. The dashed lines are a guide for eyes. The slice number *Ns* in all devices is 24.

approximately 0.15/2.6 K = 5% at a low frequency of 0.5 Hz, while for the case of high frequency, a rough evaluation indicates that the influence of friction may aggravate. To minimize the influence of friction, as mentioned above, besides thermal grease, introducing an air gap may be another choice (supplemental information S9).

These results suggest that the proposed HMR refrigerator may have excellent performance at high working frequencies. The obtained SCP of 4.9 kW/kg (ΔT_{span} = 10 K, *f* = 10 Hz) means that a maximal cooling power larger than 2.5 kW could be attained with 500 g Gd, comparable to the cooling load of a 50 m^2 building. Although the specific performance varies with different MC refrigerator systems and operating conditions, a simple comparison of maximum ΔT_{span}, SCP, and η is performed according to related MC refrigerator systems and typical AMR/PMR models. As shown in Table 1, this comparison indicates that the proposed HMR system may have high η and large cooling power, especially at a high operating frequency. It should be mentioned that another MC refrigeration technology called active MC heat pipes, which combines VC refrigeration and MC refrigeration technology, can realize a large cooling power of 12.5 kW/kg at 20 Hz but a small ΔT_{span} below 2 K because it did not possess a regenerator.[53] However, this device provided a new path to realize MC refrigeration with a large cooling power.

Impact of MCM and HTCM elements on refrigeration performances

The specific species and properties of the MCM and HTCM should also influence the regeneration process and thus the refrigeration performance. Here, we used Gd and $La(Fe_{0.92}Co_{0.08})_{11.7}Si_{1.3}$ (LFS) as MCM elements and Cu, Ag, and high thermal conductivity ALCs as HTCM elements to evaluate their impact on the performance of this HMR refrigerator. The thickness of the Gd-CL sector was set to be 0.2 mm and the ones of LFS-CL was set as 0.1 mm to keep the CL thickness in the range from $L_{MCM,1Hz}$ to $L_{MCM,5Hz}$ (*Ns* = 24) (see Figure 3D). On the basis of M-H measurements with an SQUID-VSM, the ΔT_{ad} of Gd and LFS were determined to be 4 and 1.78 K @ 1.35 T, respectively (see supplemental information S5–S8 and Figures S4–S7).

Figure 4 presents the refrigeration performance of devices composed of different MCMs and HTCMs at various structure parameters, working frequencies, and cooling loads. First, the simulation results show that the optimal U_f for the maximum R_f keeps the same value of 1.0 at a fixed frequency of 10 Hz, despite various combinations of different MCMs and HTCMs (see Figure 4A). Note here that the R_f instead of the ΔT_{span} is used in the evaluation to eliminate the influence of the discrepancy in ΔT_{ad} for different MCMs. This result confirms that the optimal U_f remains constant in this HMR refrigerator, disregarding the species of MCMs (Gd, LFS) or HTCMs (Cu, Ag, ALC). This distinctive character is attributed to the special temperature gradient in both MCM and HTCM elements, which will greatly simplify the design of the refrigerator: only the matching of the volumetric heat capacity for MCM and HTCM elements needs be considered in optimizing the efficiency of the regeneration process.

Notably, the curve of R_f versus U_f remains almost unchanged for devices composed of Gd and common HTCM elements of Cu, Ag, and ALCs (Figure 4A). Additionally, the evolution of R_f with frequency (Figure 4B) and cooling power (Figure 4C) is nearly the same for devices with these common HTCM elements. These results indicate that these three species of HTCMs have a small influence on the regeneration process in the proposed HMR refrigerators because their thermal conductivity is high enough to undertake the regeneration process (Table S1). Obviously, such characteristics would increase the chosen field of HTCM elements and decrease the difficulty of designing practical devices. Especially, considering the demands of a confined space, HTCMs with a high volumetric heat capacity would be given priority in designing miniaturized devices. Besides, because of the heat loss in the air, it never bothers to find HTCMs with higher thermal conductivity to decrease meaningless energy waste.

However, the specific MCM elements surely impact the refrigeration performance. It was further found that an R_f with LFS-MCM is larger than that with Gd-MCM at a high frequency ($f \geq 10$ Hz; see Figures 4A–4C; Table 1), indicating that LFS leads to a higher regeneration efficiency. Moreover, the device with LFS-MCM exhibits an available SCP of 9.8 kW/kg at 10 Hz, which is 18.1% larger than that with Gd-MCM (see Figures 4C and 4D), despite the latter having a larger η, 73.1%, at 1 Hz. The large volumetric heat capacity of LFS (more than twice of Gd; see Table S1) likely accounts for these results, which enables more heat to be carried and transferred within the duration of contact between the MCM and HTCM sectors in each regeneration cycle. These results suggest that MCMs with a large volumetric heat capacity would achieve a larger SCP at a high frequency. However, a high volumetric heat capacity corresponds to a relatively small thermal diffusion length (see Equation 2; Figure 3D), which means that a thin LFS-MCM layer must be used to ensure sufficient heat exchange during the regeneration. This would reduce the available ΔT_{span}. Thus, a compromise should be made in choosing MCM elements for practical device design, according to specific application scenarios.

CONCLUSION

In this paper, we propose a new conceptual HMR based on combining the principles of PMRs and AMRs, in which both HTCM and MCM elements participate in the regeneration cycle, hopefully realizing high-efficiency regeneration and refrigeration. Significantly reducing various heat losses and breaking the frequency limitation, the proposed full solid-state rotary HMR MC refrigerator holds the potential to exhibit excellent refrigeration performance superior to

traditional PMR and AMR systems, particularly at high frequency. Moreover, such full solid-state HMR designs could simplify the refrigeration performance's relation to structure parameters and endows the device with scalability to satisfy different-size refrigeration needs. Owing to the advantages mentioned above, the newly proposed HMR system offers a promising application in the field of MC refrigerators.

MATERIALS AND METHODS

See the supplemental information.

REFERENCES

1. Moore, T. An Essay on the Most Eligible Construction of Icehouses: Also, a Description of the Newly Invented Machine Called the Refrigerator (Bonsal & Niles, 1803).
2. Goetzler, W., Zong, R., Young, J., et al. (2014). Energy Savings Potential and RD&D Opportunities for Non-vapor-compression HVAC Technologies (Report, U.S. Department of Energy). www.osti.gov/biblio/1220817.
3. International Energy Agency (IEA) (2018). The future of cooling: Opportunities for energy efficient air conditioning (Report, IEA). www.iea.org/reports/the-future-of-cooling.
4. Raveendran, P.S., and Joseph Sekhar, S. (2017). Exergy analysis of a domestic refrigerator with brazed plate heat exchanger as condenser. J. Therm. Anal. Calorim. ***127***(3): 2439–2446. https://doi.org/10.1007/s10973-016-5847-2.
5. Yu, B.F., Gao, Q., Zhang, B., et al. (2003). Review on research of room temperature magnetic refrigeration. Int. J. Refrig. ***26***(6): 622–636. https://doi.org/10.1016/s0140-7007(03)00048-3.
6. The United Nations Environment Programme (UNEP), "2010 Report of the Refrigeration, Air Conditioning and Heat Pumps Technical Options Committee (RTOC). Montreal protocol on substances that deplete the ozone layer", www.unep.org/resources/report/montreal-protocol-substances-deplete-ozone-layer.
7. Shi, J., Han, D., Li, Z., et al. (2019). Electrocaloric Cooling Materials and Devices for Zero-Global-Warming-Potential, High-Efficiency Refrigeration. Joule ***3***(5): 1200–1225. https://doi.org/10.1016/j.joule.2019.03.021.
8. Chen, Y., Wang, Y., Sun, W., et al. (2022). A compact elastocaloric refrigerator. Innovation ***3***(2): 100205. https://doi.org/10.1016/j.xinn.2022.100205.
9. Romero-Muñiz, C., Law, J.Y., Revuelta-Losada, J., et al. (2023). Magnetocaloric materials for hydrogen liquefaction. Innovat. Mater. ***1***(3): 100045. https://doi.org/10.59717/j.xinn-mater.2023.100045.
10. Faehler, S., Roessler, U.K., Kastner, O., et al. (2012). Caloric Effects in Ferroic Materials: New Concepts for Cooling. Adv. Eng. Mater. ***14***(1-2): 10–19. https://doi.org/10.1002/adem.201100178.
11. Moya, X., Kar-Narayan, S., and Mathur, N.D. (2014). Caloric materials near ferroic phase transitions. Nat. Mater. ***13***(5): 439–450. https://doi.org/10.1038/nmat3951.
12. Gu, H., Qian, X.-S., Ye, H.-J., et al. (2014). An electrocaloric refrigerator without external regenerator. Appl. Phys. Lett. ***105***(16): 162905. https://doi.org/10.1063/1.4898812.
13. Zhang, T., Qian, X.-S., Gu, H., et al. (2017). An electrocaloric refrigerator with direct solid to solid regeneration. Appl. Phys. Lett. ***110***(24): 243503. https://doi.org/10.1063/1.4986508.
14. Takeuchi, I., and Sandeman, K. (2015). Solid-state cooling with caloric materials. Phys. Today ***68***(12): 48–54. https://doi.org/10.1063/pt.3.3022.
15. Manosa, L., Planes, A., and Acet, M. (2013). Advanced materials for solid-state refrigeration. J. Mater. Chem. A ***1***(16): 4925–4936. https://doi.org/10.1039/c3ta01289a.
16. Qian, X., Han, D., Zheng, L., et al. (2021). High-entropy polymer produces a giant electrocaloric effect at low fields. Nature ***600***(7890): 664–669. https://doi.org/10.1038/s41586-021-04189-5.
17. Li, B., Kawakita, Y., Ohira-Kawamura, S., et al. (2019). Colossal barocaloric effects in plastic crystals. Nature ***567***(7749): 506–510. https://doi.org/10.1038/s41586-019-1042-5.
18. Ma, R., Zhang, Z., Tong, K., et al. (2017). Highly efficient electrocaloric cooling with electrostatic actuation. Science ***357***(6356): 1130–1134. https://doi.org/10.1126/science.aan5980.
19. Qian, S., Catalini, D., Muehlbauer, J., et al. (2023). High-performance multimode elastocaloric cooling system. Science ***380***(6646): 722–727. https://doi.org/10.1126/science.adg7043.
20. Wu, J., Lu, B., Liu, C., et al. (2018). A novel cascade micro-unit regeneration cycle for solid state magnetic refrigeration. Appl. Therm. Eng. ***137***: 836–847. https://doi.org/10.1016/j.applthermaleng.2018.03.109.
21. Yu, B., Liu, M., Egolf, P.W., et al. (2010). A review of magnetic refrigerator and heat pump prototypes built before the year 2010. Int. J. Refrig. ***33***(6): 1029–1060. https://doi.org/10.1016/j.ijrefrig.2010.04.002.
22. Aprea, C., Greco, A., Maiorino, A., et al. (2018). The environmental impact of solid-state materials working in an active caloric refrigerator compared to a vapor compression cooler. Int. J. Heat Technol. ***36***(4): 1155–1162. https://doi.org/10.18280/ijht.360401.
23. Pecharsky, V.K., and Gschneidner Jr, K.A. (1997). Giant magnetocaloric effect in Gd-5(Si2Ge2). Phys. Rev. Lett. ***78***(23): 4494–4497. https://doi.org/10.1103/PhysRevLett.78.4494.
24. Pecharsky, V.K., and Gschneidner, K.A. (1997). Effect of alloying on the giant magnetocaloric effect of Gd-5(Si2Ge2). J. Magn. Magn Mater. ***167***(3): L179–L184. https://doi.org/10.1016/s0304-8853(96)00759-7.
25. Hu, F.X., Shen, B.G., Sun, J.R., et al. (2000). Great magnetic entropy change in La(Fe, M)(13)(M = Si, Al) with Co doping. Chin. Phys. ***9***(7): 550–553. https://doi.org/10.1088/1009-1963/9/7/016.
26. Brown, G.V. (1976). Magnetic heat pumping near room-temperature. J. Appl. Phys. ***47***(8): 3673–3680. https://doi.org/10.1063/1.323176.
27. Barclay, J.A., and Steyert, W.A. (1982). Active magnetic regenerator refrigeration system has piston driven through superconducting magnetic eye cylinder causing cooling through e.g. Stirling or Carnot cycle (Us Dept Energy).
28. Greco, A., Aprea, C., Maiorino, A., et al. (2019). A review of the state of the art of solid-state caloric cooling processes at room-temperature before 2019. Int. J. Refrig. ***106***: 66–88. https://doi.org/10.1016/j.ijrefrig.2019.06.034.
29. Buchelnikov, V.D., Taskaev, S.V., Bychkov, I.V., et al. (2007). The Prototype of effective device for magnetic refrigeration. In Proceedings of the Second International Conference on Magnetic Refrigeration at Room Temperature.
30. Lulu, C. (2016). Haier introduces a new solid state wine cooler at CES. https://www.digitaltrends.com/home/haier-demos-solid-state-wine-cooler-at-ces/.
31. Zhang, Y., Wu, J., He, J., et al. (2021). Solutions to obstacles in the commercialization of room-temperature magnetic refrigeration. Renew. Sustain. Energy Rev. ***143***: 110933. https://doi.org/10.1016/j.rser.2021.110933.
32. de Vries, W., and van der Meer, T.H. (2017). Application of Peltier thermal diodes in a magnetocaloric heat pump. Appl. Therm. Eng. ***111***: 377–386. https://doi.org/10.1016/j.applthermaleng.2016.09.103.
33. Silva, D.J., Ventura, J., Araújo, J., et al. (2014). Maximizing the temperature span of a solid state active magnetic regenerative refrigerator. Appl. Energy ***113***: 1149–1154. https://doi.org/10.1016/j.apenergy.2013.08.070.
34. Utaka, Y., Hu, K., Chen, Z., et al. (2019). Application of simple and effective thermal switch for solid-state magnetic refrigeration at room temperature. Appl. Therm. Eng. ***155***: 196–205. https://doi.org/10.1016/j.applthermaleng.2019.03.127.
35. Zhang, M., Momen, A.M., and Abdelaziz, O. (2016). The operating principle of a fully solid state active magnetic regenerator. In 7th International Conference on Magnetic Refrigeration at Room Temperature (Thermag).
36. Momen, A.M., Abdelaziz, O., and Vineyard, E.A. (2016). Magnetocaloric cooling system, has set of metallic rods arranged within set of channels, motor for reciprocating metallic rods between sliding extremities, and fluid exchange mechanism for directing heating and/or cooling operation.
37. Basso, V., Sasso, C.P., and Küpferling, M. (2010). A Peltier cells differential calorimeter with kinetic correction for the measurement of c(p)(H, T) and Delta s(H, T) of magnetocaloric materials. Rev. Sci. Instrum. ***81***(11): 113904. https://doi.org/10.1063/1.3499253.
38. Katter, M., Zellmann, V., Reppel, G.W., et al. (2008). Magnetocaloric Properties of La(Fe, Co, Si)(13) Bulk Material Prepared by Powder Metallurgy. IEEE Trans. Magn. ***44***(11): 3044–3047. https://doi.org/10.1109/tmag.2008.2002523.
39. Pecharsky, V.K., and Gschneidner, K.A. (1999). Magnetocaloric effect from indirect measurements: Magnetization and heat capacity. J. Appl. Phys. ***86***(1): 565–575. https://doi.org/10.1063/1.370767.
40. Fukamichi, K., Fujita, A., and Fujieda, S. (2006). Large magnetocaloric effects and thermal transport properties of La(FeSi)(13) and their hydrides. J. Alloys Compd. ***408–412***: 307–312. https://doi.org/10.1016/j.jallcom.2005.04.022.
41. Vuarnoz, D., and Kawanami, T. (2012). Numerical analysis of a reciprocating active magnetic regenerator made of gadolinium wires. Appl. Therm. Eng. ***37***: 388–395. https://doi.org/10.1016/j.applthermaleng.2011.11.053.
42. Zimm, C., Jastrab, A., Sternberg, A., et al. (1998). Description and performance of a near-room temperature magnetic refrigerator. In Joint Cryogenic Engineering/International Cryogenic Materials Conference.
43. Tura, A., and Rowe, A. (2011). Permanent magnet magnetic refrigerator design and experimental characterization. Int. J. Refrig. ***34***(3): 628–639. https://doi.org/10.1016/j.ijrefrig.2010.12.009.
44. Engelbrecht, K., Eriksen, D., Bahl, C.R.H., et al. (2012). Experimental results for a novel rotary active magnetic regenerator. Int. J. Refrig. ***35***(6): 1498–1505. https://doi.org/10.1016/j.ijrefrig.2012.05.003.
45. Romero Gomez, J., Ferreiro Garcia, R., Carbia Carril, J., et al. (2013). Experimental analysis of a reciprocating magnetic refrigeration prototype. Int. J. Refrig. ***36***(4): 1388–1398. https://doi.org/10.1016/j.ijrefrig.2013.01.008.
46. Jacobs, S., Auringer, J., Boeder, A., et al. (2014). The performance of a large-scale rotary magnetic refrigerator. Int. J. Refrig. ***37***: 84–91. https://doi.org/10.1016/j.ijrefrig.2013.09.025.
47. Yao, G.H., Gong, M.Q., and Wu, J.F. (2006). Experimental study on the performance of a room temperature magnetic refrigerator using permanent magnets. Int. J. Refrig. ***29***(8): 1267–1273. https://doi.org/10.1016/j.ijrefrig.2006.07.010.
48. Bocanegra, J.A., Scarpa, F., Bianco, V., et al. (2023). The effect of dead volumes on the performance of magnetic refrigerators. Int. J. Refrig. ***151***: 26–38. https://doi.org/10.1016/j.ijrefrig.2023.02.013.
49. Aprea, C., and Maiorino, A. (2010). A flexible numerical model to study an active magnetic refrigerator for near room temperature applications. Appl. Energy ***87***(8): 2690–2698. https://doi.org/10.1016/j.apenergy.2010.01.009.
50. Liu, M., and Yu, B. (2011). Numerical investigations on internal temperature distribution and refrigeration performance of reciprocating active magnetic regenerator of room temperature magnetic refrigeration. Int. J. Refrig. ***34***(3): 617–627. https://doi.org/10.1016/j.ijrefrig.2010.12.003.
51. Tagliafico, L.A., Scarpa, F., Canepa, F., et al. (2006). Performance analysis of a room temperature rotary magnetic refrigerator for two different gadolinium compounds. Int. J. Refrig. ***29***(8): 1307–1317. https://doi.org/10.1016/j.ijrefrig.2006.07.017.

52. Chiba, Y., Smaïli, A., Mahmed, C., et al. (2014). Thermal investigations of an experimental active magnetic regenerative refrigerator operating near room temperature. Int. J. Refrig. ***37***: 36–42. https://doi.org/10.1016/j.ijrefrig.2013.09.038.
53. Maier, L.M., Corhan, P., Barcza, A., et al. (2020). Active magnetocaloric heat pipes provide enhanced specific power of caloric refrigeration. Commun. Phys. ***3***(1): 186. https://doi.org/10.1038/s42005-020-00450-x.

ACKNOWLEDGMENTS

This work was supported by the National Key Research and Development Program of China (grant nos. 2021YFB3501202, 2020YFA0711500, 2019YFA0704900, and 2023YFA1406003), the National Natural Science Foundation of China (grant nos. 52088101, 92263202, U23A20550, and 22361132534), and the Strategic Priority Research Program (B) of the Chinese Academy of Sciences (XDB33030200). The authors are highly grateful to Prof. Bing Li of IMR CAS for providing the thermal conductivity materials of ALCs. A portion of this work was carried out at the Synergetic Extreme Condition User Facility (SECUF).

AUTHOR CONTRIBUTIONS

Y.L. designed and performed the research. Y.L., J.W., W.D., K.Q., H.Z., and T.Z. analyzed the data. Y.L., J.W., and F.H. participated in drafting and finalizing the paper. J.W., F.H., and B.S. supervised the research and secured the funds.

DECLARATION OF INTERESTS

The authors declare no competing interests.

SUPPLEMENTAL INFORMATION

It can be found online at https://doi.org/10.1016/j.xinn.2024.100645.

LEAD CONTACT WEBSITE

https://m03.iphy.ac.cn/English.htm.